A STUDY OF FLUORESCENT NANOPARTICLES: QUANTUM DOTS AND SILICA DOTS

A Thesis

Presented to the Faculty of the Graduate School

of Cornell University

In Partial Fulfillment of the Requirements for the Degree of

Master of Science

by

Diana Lynne Bull

August 2004

ABSTRACT

Optical techniques have here been employed for the study of two types of nanoscopic fluorescent probes, quantum dots and silica dots. Basic characterization of these fluorescent nanoparticles' photophysics and their capabilities have been explored utilizing the following techniques: fluorescence correlation spectroscopy, FCS, time resolved single photon counting lifetime decay measurements, and steady state absorbance, emission, and excitation measurements.

The unique properties of QDs, unmatched by any available organic fluorophore, have the potential to allow the development of FRET-based nanoscale biosensors. Unambiguous assignment of a quenching mechanism between partners as FRET may only occur through the measurement of the rate of transfer from the donor to the acceptor, this rate manifests itself as a negative amplitude component in the overall lifetime decay of the accepting partner. Two experimental regimes were executed in an attempt to identify the presence of FRET between fluorescent donor semi-conductor quantum dots surrounded by streptavidin with peak emission at 525nm (525-CdSe-ZnS QD-streptavidin) and biocytin dye acceptors chosen to have varying degrees of absorption overlap with the 525-CdSe-ZnS QD-streptavidin emission. Significant quenching of the donor, along with the acceptor, was seen when the donor was bound to the acceptor, signifying some form of energy transfer. The degree of donor quenching, illustrated by the decrease in average lifetime, corresponded with the loading ratio of the acceptor—the more acceptors present, the larger the quenching. An unambiguous assignment of the rate of transfer of excited state energy from the donor to the acceptor, signified by a negative amplitude component in the lifetime decay of the acceptor, was not accomplished.

Organic fluorescent dyes encapsulated in silica to create nanoscopic core-shell particles for use in biological applications have presented an interesting alternative to semiconductor fluorescent probes. In this experiment, an expanded core-shell morphology was surrounded by increasingly thicker layers of the siliceous shell to determine if this could control the photophysical properties of the nanoparticles. Sixteen nanoparticles were synthesized, all of distinct sizes and their photophysical properties investigated. No correlation between the thickness of the silica shell and the brightness of the particle was found. However, as the size of the particle increased the siliceous shell acted as a protective coating from potential quenchers for the TRITC dye in the center allowing molecules to stay in the triplet state for longer periods of time.

BIOGRAPHICAL SKETCH

Diana was born in Grand Junction, Colorado; she proceeded to move through most time zones in the United States. She obtained her bachelors degree in physics with a correlate in mathematics from Vassar College in the spring of 2002. In the fall of 2002 she entered the Cornell Physics program.

para raoni

ACKNOWLEDGMENTS

Even though I was only working with the Webb Group for one year, I am truly impressed by the level and caliber of science that comes out of the group...and it is not because I wouldn't know any better. It was a pleasure to work inside of a science producing machine.

First off I would like to thank Watt for taking a chance with a physicist trained in high-energy experimental physics. His counsel was always valuable. I would also like to thank Jim Alexander, without him I would have never come to Cornell in the first place. His patience, guidance, and involvement in my stay here were key to my sanity. I would also like to thank Frank Wise, who was also on my committee, for his patience and help.

Dan Larson and Harsh Vishwasrao get their own paragraph since they took countless hours instructing me on the ways of FCS and lifetime measurements respectively. I definitely did not learn enough from them...they both know too much about what they do...I am continually impressed by their breadth of knowledge and their patience. Without them I would have not known what to do with myself.

Sweng and Jie were my synthesizers and collaborators...without them I would have not had a thesis. Much thanks goes their ways.

For the rest of the science producing machine, thanks for everything. The best way to put it: simply outstanding science, simply outstanding personalities, simply not enough drinking (except the filthy, rotten, stealing, *****). Ray, Liz, Sally, Mike, Iain, Elaine, little Dan, Jesse, Joe, Jonas, Huimin, Karl, Tobias, and Val...you guys all seemed to hear about my projects and help me...I just wish I would have listened and helped you in yours! Warren, Becky....simply indispensable and patient, thank you both. And of course...Mark Williams...you just rock.

I must say...Laura and Rafael...you two have literally saved me countless times...I will soon see you in Philly (I know you will be coming!!). I don't think I could say thank you enough times to make you guys understand. John, Andrew, John...you are my boys.

I would like to thank my family...mom, missy, steve, lara, todd and dad thanks. You did what family does, you helped me out and I surely needed it.

E para meu menino...você roubou meu coração mas eu quero que você mantenha isto. Para você eu não tenho as palavras corretas para dizer obrigado.

TABLE OF CONTENTS

LIST OF FIGURES

LIST OF TABLES

LIST OF ABBREVIATIONS

A594, alexa 594 fluor biocytin

CPP, count rate per particle

EOM, electro-optic modulator

FCS, fluorescence correlation spectroscopy

FRET, fluorescence resonance energy transfer

FWHM, full-width at half max

GM, Goeppert-Maier

TRITC, tetramethylrhodamine isothiocyanate

MCP, microchannel plate

NA, numerical aperture

QD, quantum dot

QE, quantum efficiency

RET, resonance energy transfer

TEOS, tetraethylorthosilicate

TMR, tetramethylrhodamine biocytin

2P, two-photon

2PE, two-photon excitation

CHAPTER ONE

QUANTUM DOTS AS POSSIBLE FRET DONORS

INTRODUCTION

Quantum dots (QDs) are bright, photostable fluorophores that have broad excitation spectrums and size-tunable photoluminescence (PL) spectra with narrow emission bandwidths that span the visible spectrum. Cadmium selenide-zinc sulfide (CdSe-ZnS) core-shell QDs exhibit the above properties and may also be prepared with an amphiphilic polymer coating, thus allowing water solubility and bioconjugation, and hence their application to biological fields (Wu *et.al.,* 2003). To date most biological applications have focused on using QDs as fluorometeric labels in cellular imaging (Bruchez *et al*, 1998; Larson *et al.*, 2003) or for use in optical bar coding (Han *et al.,* 2001).

Recently preliminary reports of QD-QD and QD-dye-labeled biomolecule fluorescence resonance energy transfer (FRET) partners have appeared (Kagan *et al.,* 1996; Willard *et al.,* 2001; Medintz *et al.,* 2003). The possibility of using QDs in a more active role as an *in vitro* or *in vivo* biosensor through FRET is attractive as a nanoscale assembly capable of continuously monitoring target species in diverse environments while producing a useful output signal for recognition. The unique properties of QDs, unmatched by any available organic fluorophore, have the potential to allow the development of FRET-based nanoscale biosensors. A crucial aspect of FRET biosensor development involves optimizing the overlap between the donor

emission and acceptor absorption. The isotropic emission of spherical QDs eliminates orientation concerns for the donor and the acceptor by attaching several of them (Hu, 2001; Meer, 1994). The addition of many acceptors also acts to increase the FRET efficiency (Lakowicz, 1999).

Unambiguous assignment of a quenching mechanism between partners as FRET may only occur through quantifying the rate of transfer of excited state donor energy to the acceptor; the time of energy transfer appears with a negative amplitude signifying the transfer of energy from the donor to the acceptor (Meer, 1994). This explicit measurement has failed to appear in the literature to date, and hence it is still unknown if QDs are truly acting as a donor in these systems, or if some other form of energy transfer is responsible for quenching the quantum dot. Here two experimental regimes were executed in an attempt to identify the presence of FRET between fluorescent 525-CdSe-ZnS QD-streptavidin donor and biocytin dye acceptors with varying degrees of overlap. Figure 1.1 illustrates the overlap between the QD-donor and the acceptors—Alexa 594 Fluor biocytin (A594) and tetramethylrhodamine biocytin (TMR). Time resolved single photon counting lifetime measurements were obtained for both the donor and the acceptor in two loading ratios under the following conditions: 1) donor in absence of acceptor, 2) acceptor in absence of donor, 3) donor bound to biocytin in absence of acceptor, 4) donor and acceptor present in absence of binding protein, and 5) donor bound to acceptor.

Significant quenching of the donor was seen when the donor was bound to the acceptor, signifying some form of energy transfer. Quenching of the acceptor was also seen under these conditions. The degree of donor quenching, illustrated by the decrease in average lifetime, corresponded with the loading ratio of the acceptor—the more acceptors present, the larger the quenching. An unambiguous assignment of a negative amplitude component with the time of transfer on the acceptor lifetime decay

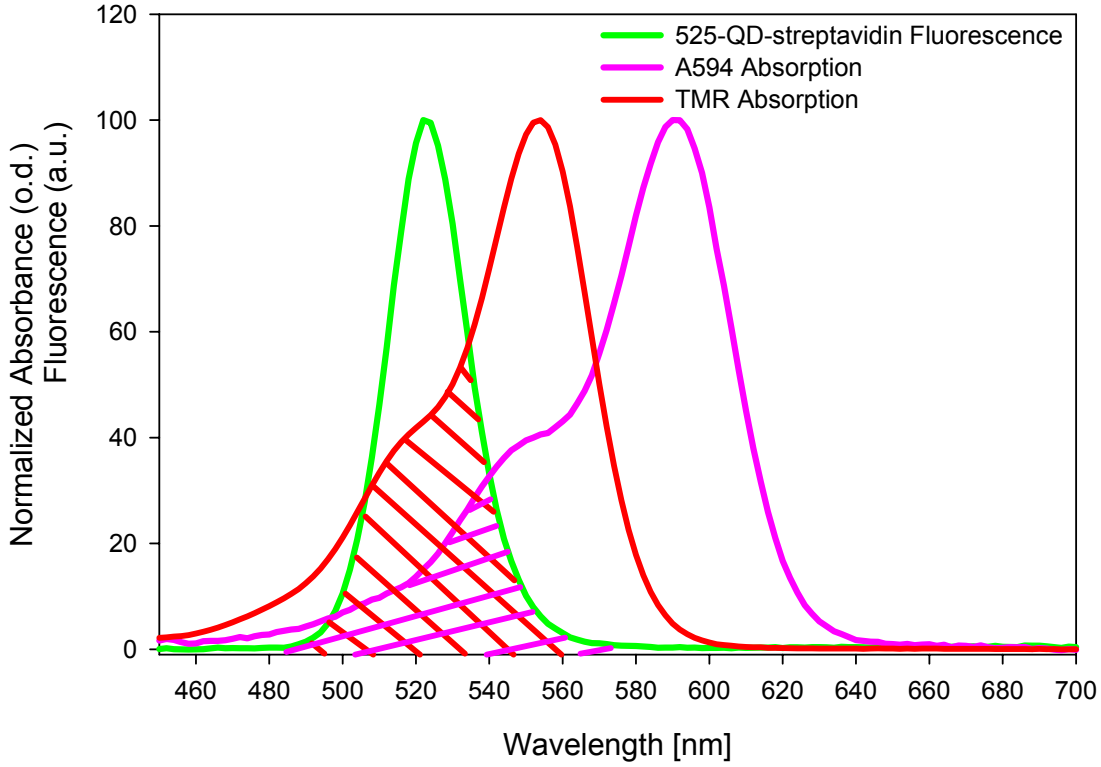

Figure 1.1: Steady State Spectroscopy of QD-donor Emission and Acceptors' Absorbance. TMR-acceptor absorbance is shown in red and will from here on be represented by the color red. A594-acceptor absorbance is shown in pink and will from here on be represented by the color pink. The red and pink fill lines are attempting to illustrate the overlap of the donor emission with the acceptor absorbance. As can be seen, TMR has a stronger overlap with the donor than A594 does.

was not accomplished; however, the residuals seem to imply that something is not being modeled correctly in the multiexponential fit. All of the control conditions yielded the expected results; an increase in the lifetime of the QD with biocytin present and comparable lifetimes for the donor and acceptor when not bound to the pure runs.

MATERIALS AND METHODS

Sample labeling and purification. All sample synthesis procedures were carried out by Jie Yao. Qdot525-streptavidin was purchased from Quantum dot Corp. (Hayward, CA), and labeled with Alexa594-biocytin and TMR-biocytin (Molecular Probes). For every QD-streptavidin sample, average biotin binding sites on each QD were determined to be around 30-60 by fluorescence quenching experiments performed by Jie Yao. 0.1uM QD-streptavidin solution was mixed with biotin-dye at different loading ratio (1:10 and 1:50) at room temperature for 30 minutes. Conjugates were purified by Microcon-100 spin column (Millipore).

Absorbance. Absorbance measurements were done with a Cary 300 Bio UV/VIS dual beam spectrophotometer. Measurements were taken in 2nm step intervals from 450-700nm with a dwell of 1 sec on each interval.

Time Resolved Spectroscopy. A mode-locked Ti:sapphire laser system (Tsunami; Spectra Physics) pumped by an Ar^{+}-laser (Spectra Physics) was used to generate femtosecond laser pulses in the 790 nm range with pulse width of ~100fs. For these measurements the repetition rate of the laser was reduced to 10 MHz using an electro-optic modulator, EOM, (Conoptics) due to the long lifetime of the quantum dot. The light was focused on the sample with a 40x, 1.15 NA objective, and filtered two-photon (2P)-fluorescence was imaged on a microchannel plate MCP photomultiplier tube, PMT, (Hamamatsu) at the magic angle of 39º with respect to the laser. The

magic angle was utilized in order to eliminate rotational effects on the measured fluorescence decays. For fluorescence collection from the donor, both blue glass and a 515±15nm bandpass filter were used; for acceptor collection both a 620±50nm bandpass filter and a 575±75nm bandpass filter were used; a 720nm short pass filter was in place for all measurements. The fluorescence was pre-amplified (Stanford Research Systems, Inc.) and then counted using a gated photon counter (Stanford Research Systems, Inc.). The laser intensity was varied using a calibrated neutral density filter wheel (New Focus, Inc.). The SPC-730 (Becker & Hickl) module was installed in, and controlled by, a personal computer that was also used for data storage. The instrument response function was measured regularly at a right angle with respect to the laser and used for deconvolution in the fitting routines.

Due to the remarkably large 2PE-cross section of quantum dots the average power of the excitation laser at the sample was kept very low, ~1mW, in order to predominantly excite the donor and not the acceptor. At ~800nm the 2P cross-section is ~7000GM for the 525-CdSe-ZnS QD, ~100GM for A594, and ~100GM for rhodamine, a close relative of TMR. With a factor of ~70 separating the donor excitation probability from the acceptor excitation probability, it was expected that the donor would be the predominantly excited species. The low excitation power was also necessary to keep the count rates low, below 0.5 kHz, in order to avoid pulse pile-up effects and saturation of the MCP (O'Connor and Phillips, 1984). Each measurement was run for one hour. The use of double filters helped to minimize fluorescence bleedthrough, thus allowing different time scales to be utilized for the donor and acceptor time resolved lifetime measurements. This was advantageous due to the expected transfer rates yielding small decay components and small amplitude contributions in the acceptors lifetime when undergoing FRET. The acceptor dye's lifetime was recorded at higher resolution (2.44ps vs. the 6.10ps resolution used for

the donor decays) thus allowing for characterization of smaller decay time constants. The fluorescence decays were fit using two versions of Becker & Hickl SPCImage decay fitting software, one written to be capable of fitting negative amplitudes and the other a more reliable and older version. They were also fit using a fitting program developed at Cornell University by Harsh Vishwasrao in MATLAB, this program searched for a global minimum using the fminsearch function. The functional form used to fit the decay curves in all instances was:

$$F(t) = F_{baseline} + F_o \bullet \sum_{i=1}^{n} a_i \exp(-(t - t_o)/\tau_i) \tag{1.1}$$

where n is the number of components; the decay time constants are τ_i; the amplitudes are a_i; $F_{baseline}$ is the baseline fluorescence and F_o is the peak fluorescence at time t_o, where t_o is the temporal offset of the fluorescence decay. The fitting routine effectively deconvolved the measured system response function. The amplitudes (a_i) satisfy the condition that $\sum_{i=1}^{n} a_i = 1$ and the average lifetime $< \tau >$ is given by:

$$< \tau >= \sum_{i=1}^{n} a_i \tau_i \Big/ \sum_{i=1}^{n} a_i \tag{1.2}$$

FRET Calculations. The distance between the donor and acceptor at which half the excitation energy of the donor is transferred to the acceptor while the other half is dissipated by all other processes is the Förster distance R_o. Resonance energy transfer (RET) only involves the coupling of the emission transition moment of the donor and the absorption transition moment of the acceptor. Since the electric dipole is the first term in a multipole expansion of an electrically neutral system, RET involves the transition dipoles of the donor and acceptor, to first order. The transition dipole is a result of the interaction of light with matter; the light's electric field induces dipolar moments which govern the magnitude of the transition probabilities between two states (Cantor and Schimmel, 1980). The rate of transfer is thus governed by the degree of dipole-dipole coupling, and in terms of measurable and calculable quantities it is given by:

$$k_T = (1/<\tau_D>)(R_o/r)^{-6} \tag{1.3}$$

where $<\tau_D>$ is the average lifetime of the donor without the acceptor, R_o is the Förster distance, and r is the distance between the donor and acceptor. Both the rate and the efficiency of transfer, E, have the $1/r^6$ dependence characteristic of long-range dipole-dipole interactions. The efficiency of transfer, E, is given by:

$$E = 1 - Q_{DA}/Q_D = R_o^6/(R_o^6 + r^6) \tag{1.4}$$

where Q_{DA} is the quantum yield of the donor with the acceptor attached, Q_D is the quantum yield of the donor alone, and r is the distance between the donor and acceptor. The donor and acceptor need to be relatively close to each other, ~10-100Å, but their separation distance is truly dictated by their Förster distance. The Förster distance, R_o, may be calculated for a donor-acceptor pair through the following formula:

$$R_o^6 = (9000(\ln 10)\kappa^2 Q_D J)/(128\pi^2 n^4 N_{AV}) \tag{1.5}$$

where κ^2 is the orientation factor between the two transition dipoles, Q_D is the same as above, J is the degree of overlap between the donor emission spectrum and the acceptor absorption spectrum, n is the index of refraction of the medium, and N_{AV} is Avogadro's number. The overlap integral, J, is calculated via the molar extinction coefficient of the acceptor, $\varepsilon_A(\lambda)$, and the fluorescence of the spectrum of the donor, $f_D(\lambda)$, normalized on the relevant wavelength scale in the following manner:

$$J = \int_0^\infty f_D(\lambda)\varepsilon_A(\lambda)\lambda^4 d\lambda. \tag{1.6}$$

Where $f_D(\lambda)$ is given by the corrected donor fluorescence intensity in the wavelength range λ to $\lambda + \Delta\lambda$ with total intensity normalized to unity.

RESULTS

A594 has a molar extinction coefficient of 79,900$M^{-1}cm^{-1}$ at 591nm in buffer at pH7 (Molecular Probes), and this value was utilized to calculate $\varepsilon_{A594}(\lambda)$. Using

Eq. 1.6, the overlap integral, J, was calculated to be $12.*10^{15}nm^4M^{-1}cm^{-1}$ for one A594 fluorophore with one QD. TMR has a molar extinction coefficient of $103{,}000M^{-1}cm^{-1}$ at 554nm in buffer at pH7 (Molecular Probes) thus yielding an overlap integral value of $38.*10^{15}nm^4M^{-1}cm^{-1}$. The quantum yield of the 525-CdSe-ZnS QD with streptavidin was found to be 57.± 4.0% by Jie Yao. It was assumed that both the donor and the acceptor were free to reorient their transition dipoles rapidly on the time scale of fluorescence emission, thus κ^2 was taken to be its limiting value of 2/3. Thus, for the A594-QD pair an R_o value of 48Å was calculated and for the TMR-QD pair an R_o value of 59Å was obtained.

Under the assumption of isotropic attachment, emission, and absorption, the quantitative effect on the FRET efficiency of having multiple acceptors for each QD donor can be estimated by:

$$E = nR_o^6 / (nR_o^6 + r^6) \tag{1.7}$$

where n is the number of acceptor molecules (Frederix, 2002 and Lakowicz, 1999). In Eq 1.7 it is assumed that each acceptor is the same distance from the donor, that the donor interacts with each acceptor independently, that the acceptors do not interact with each other, and that all orientation issues are taken into account in κ^2 (Frederix, 2002). From x-ray-crystallography data, the size of a biotin complex is ~54Å, from QD Corporation (Qdot) the radius of the QD-streptavidin complex, from the center to the edge of the streptavidin, was found to be ~75Å via transmission electron microscopy, TEM. However, in order to successfully make a TEM measurement, the sample must be dried; in this process the QD is reduced in size by approximately half. If one does not dismiss the effects of QD swelling, then the center to biotin edge distance is approximately 244Å (from FCS data taken by Jie Yao); this separation distance reduces all of the efficiencies to fractions of a percent, these are not resolvable values. However, if one allows for the possibility that the transition

moment can be modeled from a place other than the center of the QD, then, even the effects of the swelling of the QD, FRET efficiencies could achieve resolvable values.

The TEM data will be used here to model the system, in doing this there is the base assumption that if a FRET component is found in the lifetime decay of the acceptor, the coupling of the two dipoles is occurring from a place other than the center of the core of the QD. Thus, if one assumes that the transition moment of the donor is located at the center of the QD, to obtain the largest separation distance under dried conditions, then the distance between the donor and acceptor molecule is at most ~129Å. If only one acceptor were present per donor, than, for this system, a donor-acceptor separation distance should be around 60-70Å to achieve an efficiency of 20%. However, since high loading ratios are being used, this distance, in the case of the 1:10 ratio, increases from 60-75Å to approximately 90-110Å.

Thus, for the A594-QD with separation distance of 129Å efficiency of 2.6% and 12% would occur for the 1:10 and 1:50 loading ratios respectively. For the TMR pair with the same separation distance, the efficiencies increase to 8.4% and 31% for the 1:10 and 1:50 loading ratios respectively.

With these efficiencies, a negative amplitude component in the acceptor decay was expected to be present for the higher loading ratios, and larger for the TMR acceptor if the coupling of dipoles occurred from a place other than the center of the QD. Each lifetime decay has been fit with multiple programs attempting to identify a negative amplitude with the transfer time decay constant in the acceptor decay unambiguously. The following quoted values were obtained from SPCImage Version 2.6.0 allowing for scattered light in the fit. After attempting to fit these curves in other programs and noticing a large amplitude corresponding to a small time constant component in some of the fits, often indicating a scattering of the excitation light, this program was used due to its ability to accurately model scatter.

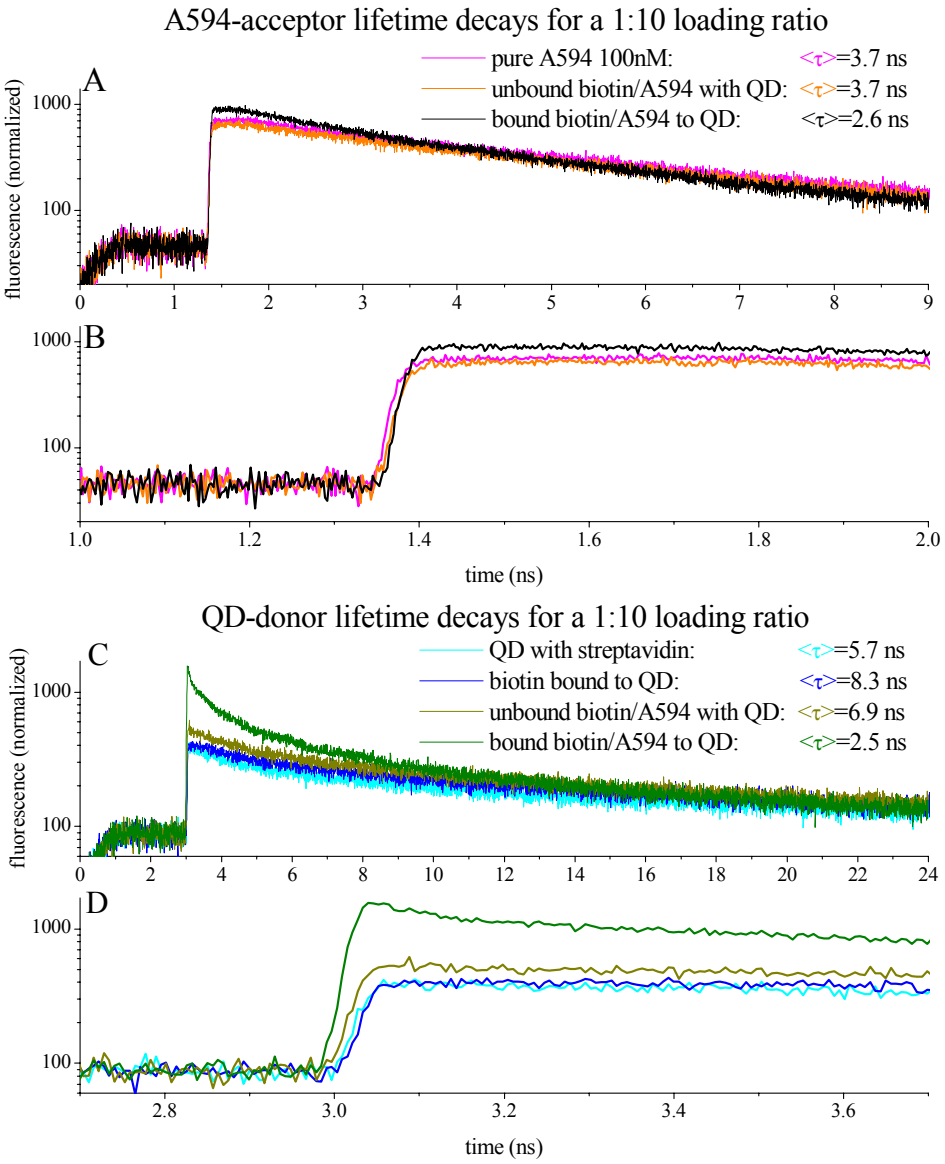

Figure 1.2: Time Resolved Fluorescence of A594-acceptor and QD-donor in a 1:10 Ratio. These decays are normalized by the intensity of the run, length of the run and to one of the decays. A) Fluorescence of decays of A594-acceptor 1) by itself (pink) 2) with the QD-donor present, but unbound (orange) and 3) when bound to the QD-donor (black). B) A close-up of the initial rise region from A) where one would expect to find the negative amplitude. C) Fluorescence decays of QD-donor 1) by itself (cyan) 2) bound to biotin (blue) 3) with the A594-acceptor present, but unbound (brown) 4) when bound to the A594-acceptor (green). D) A close-up of the initial rise region from C). The average lifetime values are given in the legend for each lifetime decay.

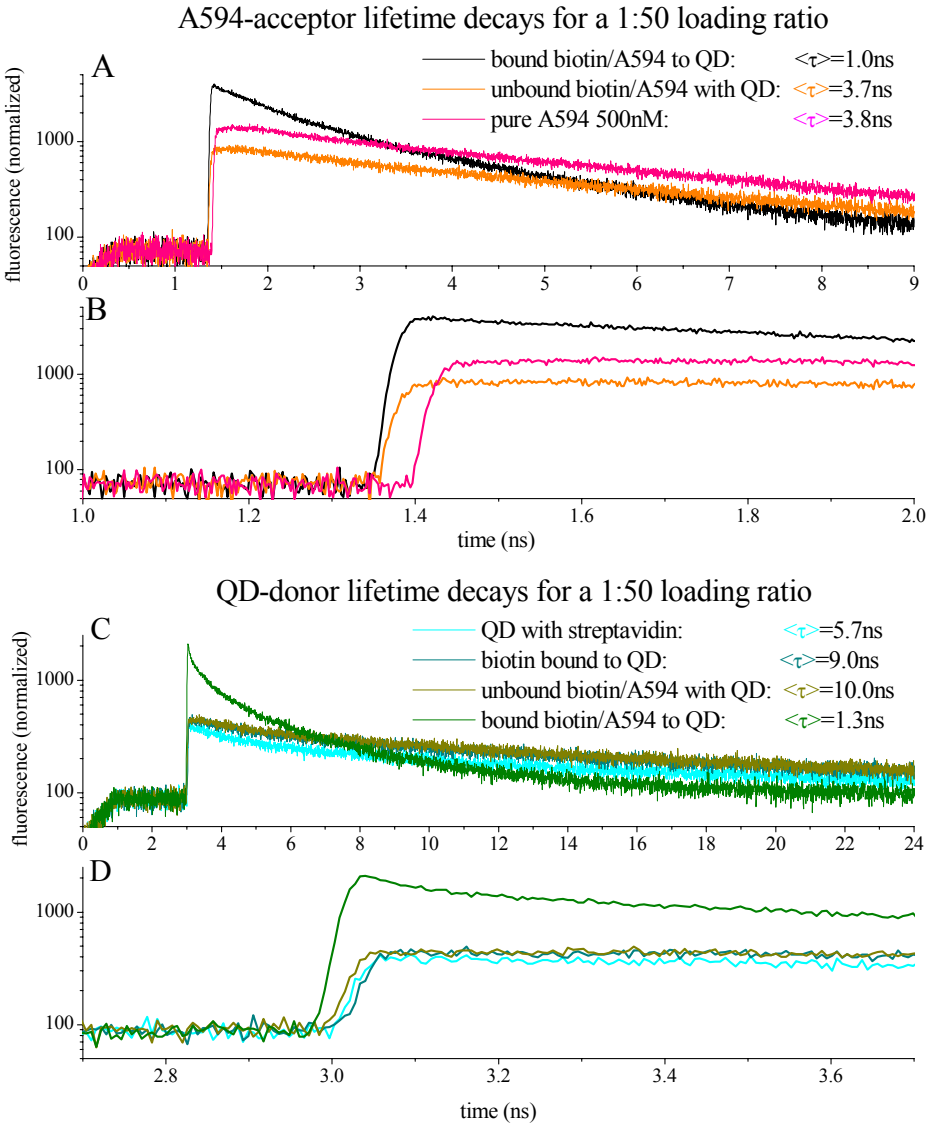

Figure 1.3: Time Resolved Fluorescence of A594-acceptor and QD-donor in a 1:50 Ratio. These decays are normalized by the intensity of the run, length of the run and to one of the decays. A) Normalized fluorescence of decays of A594-acceptor 1) by itself (pink) 2) with the QD-donor present, but unbound (orange) and 3) when bound to the QD-donor (black). B) A close-up of the initial rise region from A) where one would expect to find the negative amplitude. C) Normalized fluorescence decays of QD-donor 1) by itself (cyan) 2) bound to biotin in a 1:10 ratio (blue) 3) with the A594-acceptor present, but unbound (brown) 4) when bound to the A594-acceptor (green). D) A close-up of the initial rise region from C). The average lifetime values are given in the legend for each lifetime decay.

Table 1.1: Compiled Time Resolved Values for A594-acceptor and QD-donor in a 1:10 Ratio. a_i is the amplitude of the τ_i component; $<\tau>$ is the average lifetime; the scatter time component represents a distortion component in the decay; 2σ is 84.9% of FWHM of the response function. All time values are in ps. The green columns are the lifetime components for the QD-donor while the pink columns are the lifetime components for the A594-acceptor.

Lifetime decay parameters	biotin bound to QD	unbound biotin/A594 with QD	bound biotin/A594 to QD	A594 100nM	unbound biotin/A594 with QD	bound biotin/A594 to QD
a_1	0.45	0.46	0.58	0.34	0.46	0.29
τ_1	500	520	280	1800	2300	780
a_2	0.31	0.23	0.25	0.66	0.54	0.71
τ_2	6000	4600	2100	4700	5000	3300
a_3	0.24	0.31	0.17			
τ_3	26000	18000	11000			
$<\tau>$	**8300**	**6900**	**2500**	**3700**	**3700**	**2600**
Scatter in ps	0.00	0.00	47	7.0	9.0	18
2σ of the response function	37	38	38	32	34	34

Table 1.2: Compiled Time Resolved Values for A594-acceptor and QD-donor in a 1:50 Ratio. a_i is the amplitude of the τ_i component; $<\tau>$ is the average lifetime; the scatter time component represents a distortion component in the decay; 2σ is 84.9% of FWHM of the response function. All time values are in ps. The green columns are the lifetime components for the QD-donor while the pink columns are the lifetime components for the A594-acceptor.

Lifetime decay parameters	Biotin bound to QD	Unbound biotin/A594 With QD	Bound biotin/A594 to QD	A594 500nM	Unbound biotin/A594 with QD	Bound biotin/A594 to QD
a_1	0.44	0.36	0.61	0.41	0.28	0.32
τ_1	490	660	240	2400	1800	140
A_2	0.31	0.35	0.27	0.59	0.72	0.38
τ_2	6700	7500	1700	4800	4500	730
A_3	0.25	0.29	0.12			0.30
τ_3	27000	26000	5600			2300
$<\tau>$	**9000**	**10000**	**1300**	**3800**	**3700**	**1000**
Scatter in ps	0.00	0.00	64	17	8	40
response function 2σ	37	38	38	33	34	34

For the 525-CdSe-ZnS QD with streptavidin a $<\tau>$ of 5.7ns was obtained. Once biotin was attached to the streptavidin, the lifetime of the QD increases to 8.3ns and 9.0ns for the 1:10 and 1:50 loading ratios respectively most likely due to the sheltering effect of the biotin. No short time decay component was evident when the biotin was attached to the QD indicating that the short time constant was not due to the biotin-streptavidin bond.

The inverse of Eq 1.3 yields the expected time decay constant for the negative amplitude component in the total decay. When using the average lifetime of the quantum dot when attached to the biotin, the relevant comparison basis, and the separation distance of 129Å, time constants on the order of tens of picoseconds were found. The A594 acceptor was expected to have time decay components from the transfer of energy of 22ps and 24ps for the 1:10 and 1:50 loading ratios respectively. While the TMR acceptor was expected to have time decay components from the transfer of energy of 76ps and 83ps for the 1:10 and 1:50 loading ratios respectively. Obviously, the TMR values are much larger, again due to the larger overlap, which is related to the strength of the dipole-dipole coupling, of the TMR with the 525-CdSe-ZnS QD-streptavidin. The resolution of the fits, however, is truly limited by the response function of the system. Conservatively, one can not identify a time component that is smaller than twice the width of the response function. Typically for this system a response function on the order of 40ps is obtained, thus only the TMR would have FRET time decay constants that could be confidently resolved.

Figure 1.2 and Figure 1.3 illustrate the A594-acceptor and QD-donor lifetime decays. These decays are normalized by the intensity of the run, length of the run and to the free dye or pure QD respectively. As can be easily seen in panels A and C for both figures, the lifetime of the pair when bound together decreases dramatically for the QD and also for the A594. Panels B and D zoom in on the initial rise region of the

curve where the negative amplitude and the scattering component would be present. In Fig 1.3 D, the fast time-decay component is clearly visible for the bound biotin/A594-QD complex, it is the fast decay component visible directly after the initial rise. The weighted average decay times $<\tau>$ for each of the curves is shown in the legends of Fig. 1.2 and 1.3 A and C.

Tables 1.1 and 1.2 list the lifetime decay parameters from the SPCImage fits for the A594-QD pair. The 2σ width of the corresponding response function used for deconvolution is also listed. When scatter was allowed for, all residuals in the figures below were flat thus signifying that the curve had been modeled correctly. The short time constant, or scatter component, is negligible until the acceptor is actually bound to the donor, and then it manifests itself in both the donor and acceptor decays. Also in Table 1.3 the A594, when bound to the QD, requires a third decay component to accurately model the lifetime decay.

Figure 1.4 and Figure 1.5 illustrate the TMR-acceptor and QD-donor lifetime decays. These decays are also normalized by the intensity of the run, length of the run and to the free dye or pure QD respectively. Again, as seen in panels A and C of both figures, the lifetime of the pair when bound together decreases dramatically for the QD and also for the TMR, much more dramatically than for the A594-QD pair. This larger decrease in the lifetime is most likely due to the larger overlap that TMR possesses with the QD. Panels B and D zoom in on the initial rise region of the curve where the negative amplitude and the scattering component would be present. No scattering component is clearly visible in these panels. The weighted average decay times $<\tau>$ for each of the curves is shown in the legends of Fig. 1.2 and 1.3 A and C respectively.

Tables 1.3 and 1.4 list the lifetime decay parameters from the SPCImage fits for the TMR-QD pair. The 2σ width of the corresponding response function used for

deconvolution is also listed. When scatter was allowed for, not all residuals in the figures below were flat, thus signifying that the curve had not been modeled correctly. In particular, for the 1:50 QD-TMR pair, at the location of the initial rise of the curve the residuals could not be smoothed out. It is not necessary that this actually be a negative component, however this curve was expected to be the most likely to have one. Again, the short time component is negligible until the acceptor is actually bound to the donor and then it manifests itself in both the donor and acceptor decays. An extra decay component again appears in the acceptor decay once the donor is bound.

DISCUSSION

It has been shown that a partner fluorophore quenches a QD, however, it has not been proven that this mechanism proceeds via resonantly transfered energy (FRET). Partners exhibiting strong overlap were chosen as the acceptors for the QD-donor, and they were attached at a high loading ratio to increase the FRET efficiency. However, no negative amplitude could be fit to the lifetime decay of the acceptor molecule most likely due to the following parameters: the direct excitation of the acceptor, the strong short time decay component, and the large distances between the partners.

Due to the inability to excite only the donor fluorophore without exciting the acceptor pairs, the acceptor fluorescence decay curves are mainly composed of strong initial excitation signal. This strong excitation signal complicates and overpowers the weaker indirect excitation from energy transfer, thus making the negative amplitude an elusive component in the curve. Since the 2PE-cross sections were unknown for the acceptor dyes, it was not possible to select an appropriate excitation wavelength nor was it possible to quantify the amount that the acceptors were directly excited.

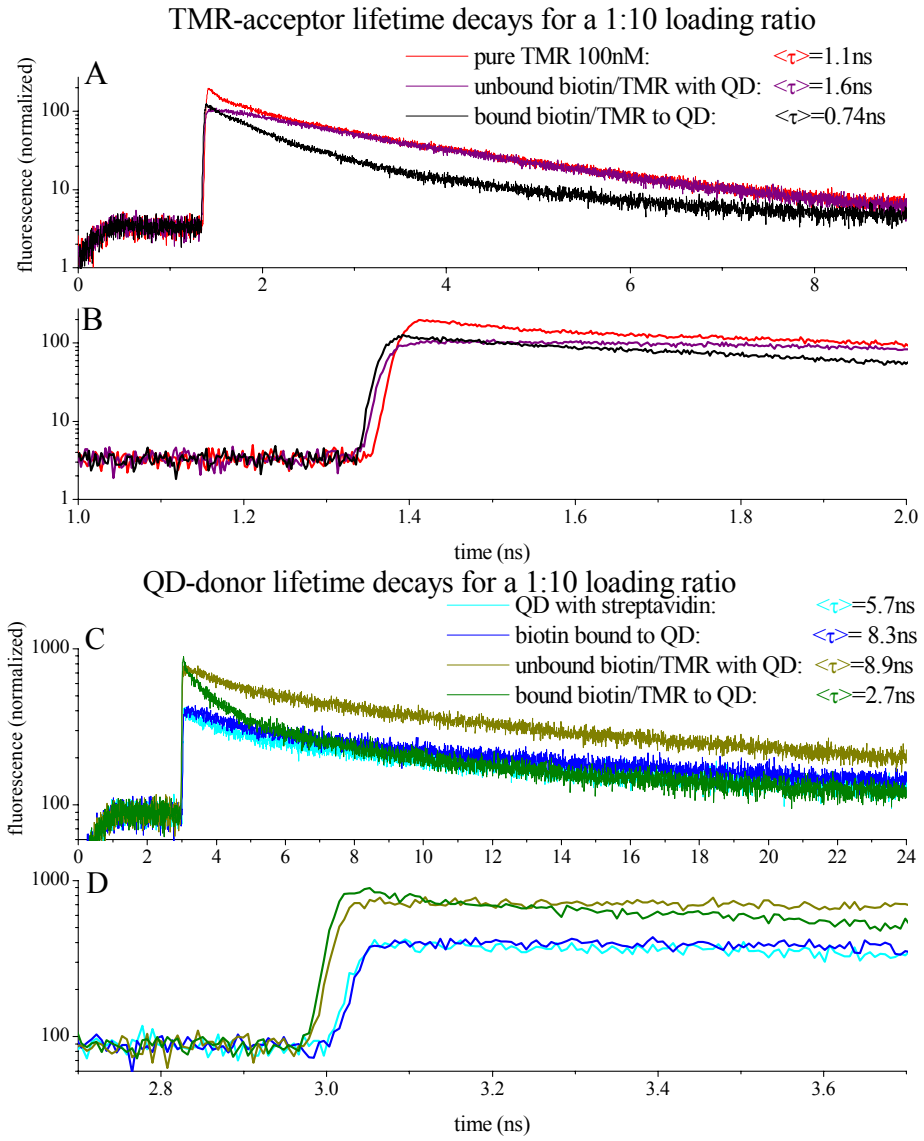

Figure 1.4 : Time Resolved Fluorescence of TMR-acceptor and QD-donor in a 1:10 Ratio. These decays are normalized by the intensity of the run, length of the run and to one of the decays. A) Normalized fluorescence of decays of TMR-acceptor 1) by itself (red) 2) with the QD-donor present, but unbound (purple) and 3) when bound to the QD-donor (black). B) A close-up of the initial rise region from A) where one would expect to find the negative amplitude. C) Normalized fluorescence decays of QD-donor 1) by itself (cyan) 2) bound to biotin in a 1:10 ratio (blue) 3) with the TMR-acceptor present, but unbound (brown) 4) when bound to the TMR-acceptor (green). D) A close-up of the initial rise region from C). The average lifetime values are given in the legend for each lifetime decay.

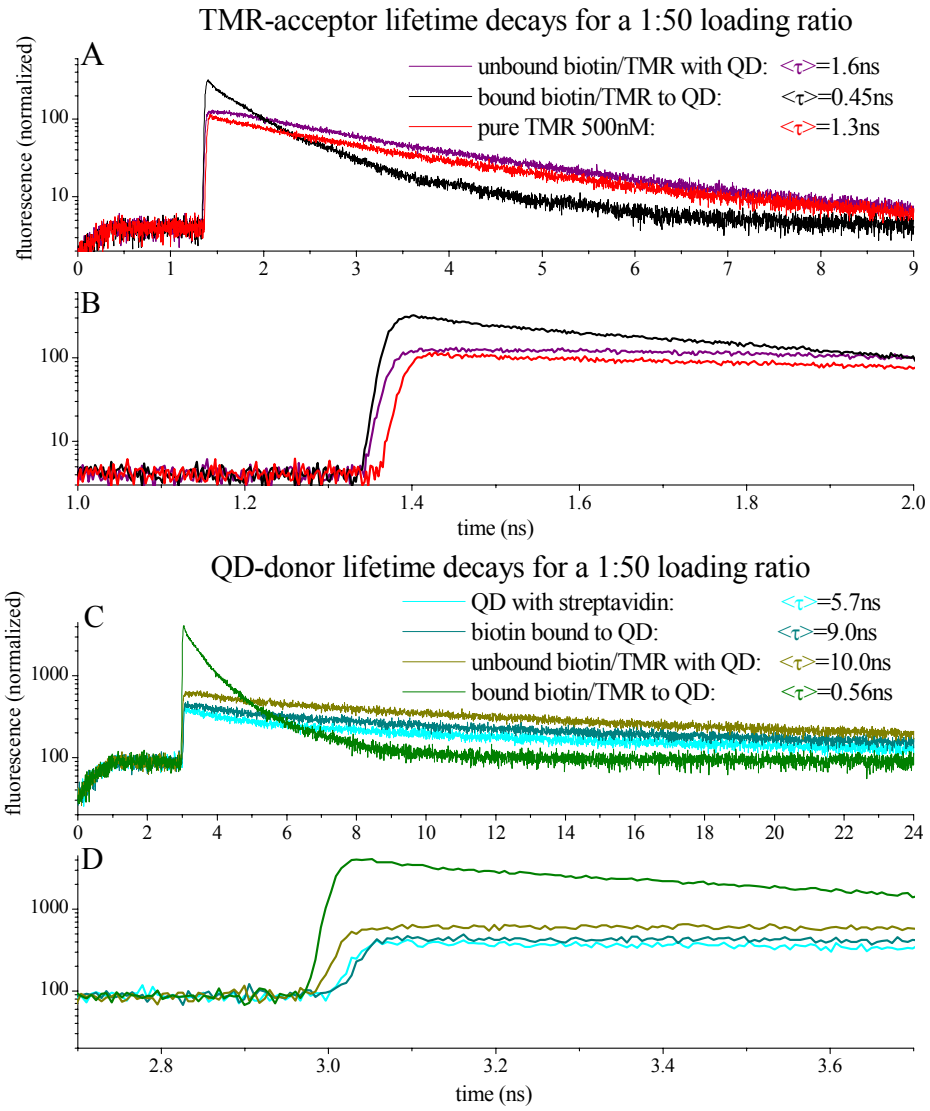

Figure 1.5: Time Resolved Fluorescence of TMR-acceptor and QD-donor in a 1:50 Ratio. These decays are normalized by the intensity of the run, length of the run and to one of the decays. A) Normalized fluorescence of decays of TMR-acceptor 1) by itself (red) 2) with the QD-donor present, but unbound (purple) and 3) when bound to the QD-donor (black). B) A close-up of the initial rise region from A) where one would expect to find the negative amplitude. C) Normalized fluorescence decays of QD-donor 1) by itself (cyan) 2) bound to biotin in a 1:10 ratio (blue) 3) with the TMR-acceptor present, but unbound (brown) 4) when bound to the TMR-acceptor (green). D) A close-up of the initial rise region from C). The average lifetime values are given in the legend for each lifetime decay.

Table 1.3: Compiled Time Resolved Values for TMR-acceptor and QD-donor in a 1:10 Ratio. a_i is the amplitude of the τ_i component; $<\tau>$ is the average lifetime; the scatter time component represents a distortion component in the decay; 2σ is 84.9% of FWHM of the response function. All time values are in ps. The green columns are the lifetime components for the QD-donor while the red columns are the lifetime components for the TMR-acceptor.

Lifetime decay parameters	biotin bound to QD	unbound biotin/TMR with QD	Bound biotin/TMR to QD	TMR 100nM	Unbound biotin/TMR with QD	bound biotin/TMR to QD
a_1	0.45	0.43	0.60	0.51	0.24	0.44
τ_1	500	630	350	240	290	160
A_2	0.31	0.33	0.24	0.49	0.76	0.43
τ_2	6000	7000	2400	2100	2000	750
A_3	0.24	0.24	0.16			0.13
τ_3	26000	26000	12000			2700
$<\tau>$	**8300**	**8900**	**2700**	**1100**	**1600**	**740**
Scatter in ps	0.00	0.00	23	52	0.00	33
Response function 2σ	37	35	35	33	32	32

Table 1.4: Compiled Time Resolved Values for TMR-acceptor and QD-donor in a 1:50 Ratio. a_i is the amplitude of the τ_i component; $<\tau>$ is the average lifetime; the scatter time component represents a distortion component in the decay; 2σ is 84.9% of FWHM of the response function. All time values are in ps. The green columns are the lifetime components for the QD-donor while the red columns are the lifetime components for the TMR-acceptor.

Lifetime decay parameters	biotin bound to QD	unbound biotin/TMR with QD	Bound biotin/TMR to QD	TMR 500nM	Unbound biotin/TMR with QD	Bound biotin/TMR to QD
a_1	0.44	0.37	0.74	0.38	0.25	0.51
τ_1	490	610	290	180	260	140
A_2	0.31	0.35	0.22	0.62	0.75	0.38
τ_2	6700	7700	1100	2000	2000	540
A_3	0.25	0.28	0.04			0.11
τ_3	27000	27000	2800			1500
$<\tau>$	**9000**	**10000**	**560**	**1300**	**1600**	**450**
Scatter in ps	0.00	6	86	20	0.00	74
response function 2σ	37	35	35	35	32	32

The appearance of the short time component term, or possibly a scatter term, in the bound pairs has also contributed to the concealing of a negative amplitude term. Since no short time component is present when the biotin is bound to the quantum dot, the presence of the biotin cannot be the root of the short time component. However, once the acceptor and the donor are bound, this short time component arises, and quite strongly. The origin and meaning of this state is unknown at this time, and it must be dealt with in future experiments.

As has been seen in the literature (Medintz *et al.,* 2003), the binding of the donor fluorophore to the acceptor has resulted in significant quenching of the donor. Interestingly, the acceptor is also quenched in this situation, most likely due to the fact that many acceptors are in close vicinity around the dot. This situation easily lends itself to significant quenching. The acceptor also obtains another decay pathway. The existence of this additional pathway may shed light on the type of energy transfer occurring between the donor and acceptor. One control experiment has been left out of the experiment, and it has to do exactly with this issue. It must be determined if the extra decay pathway is an artifact of the streptavidin-biotin bound state, or if arises only when the donor and acceptor are in thier bound state. However, analysis of this situation is beyond the scope of this experiment.

The strong overlap integral between the donor and acceptors and the high quantum yield of the QD-donor present favorable conditions for FRET. However, due to the size of the QD-donor it would be necessary to model the transition moment of the QD-donor from the edge of the CdSe core or from the ZnS shell in order to achieve reasonable efficiencies. To accurately model a transition moment from anywhere but the center of the QD would require knowledge of the swelling mechanism in the QD. Thus, the detection of a negative amplitude could be most

easily achieved by using a smaller QD and by choosing an excitation wavelength that would minimally excite the acceptor.

CONCLUSION

Due to the unparalleled properties of quantum dots, their use as FRET partners for biosensing is extremely attractive. However, their ability to resonantly transfer their excited state energy to a partner will continue to be debatable until the acceptor's negative amplitude is seen. Medintz (Medintz *et al.*, 2003) presents compelling evidence that a quantum dot can act as a donor in FRET, however, recognition by the authors is given that without measurement of the negative amplitude their results are disputable.

REFERENCES

Bruchez, M., J.M. Moronne, P. Gin, S. Weiss, and A.P. Alivasatos. 1998. Semiconductor nanocrystals as fluorescent biological labels. *Science*. 281:2013-18.

Cantor, C.R. and P.R. Schimmel. *Biophysical Chemistry Part II: Techniques for the study of biological structure and function.* (W.H. Freeman and Company, New York, 1980).

Frederix, P.L.T.M., E.L. de Beer, W. Hamelink, and C.G. Gerritsen. 2002. Dynamic Monte Carlo Simulations to model FRET and photobleaching in systems with multiple donor-acceptor interactions. *J. Phys. Chem. B*. 106:6793-801.

Han, M.Y., X.H. Gao, J.Z. Su, and S. Nie. 2001. Quantum-dot-tagged microbeads for multiplexed optical coding of biomolecules. *Nature Biotchnol.* 19:631-35.

Hu, J.T., L. Li, W. Yang, L. Manna, L. Wang, A.P. Alivasatos. 2001. Linearly Polarized Emission from Colloidal Semiconductor Quantum Rods. *Science*. 292:2060-63.

Kagan, C.R., C.B. Murray, and M.G. Bawendi. 1996. Long-range resonance energy transfer of electronic excitations in close-packed CdSe quantum-dot solids. *Phys. Rev. Lett.* 76:1517-20.

Lakowicz, J.R. *Principles of Fluorescence Spectroscopy* 2nd edn (Kluwer Academic, New York, 1999).

Larson, D.R., W.R. Zipfel, R.M. Williams, S.W. Clark, M.P. Bruchez, F.W. Wise, W.W. Webb. 2003. Water-Soluble Quantum Dots for Multiphoton Fluorescence Imaging in Vivo. *Science.* 300:1434-36.

Meer, B.W. van der, G. Coker III, S.-Y.S. Chen. *Resonance Energy Transfer: Theory and Data*. (VCH, New York, 1994).

Medintz, I.L., A.R. Clapp, H. Mattoussi, E.R. Goldman, B. Fisher, J.M. Mauro. 2003. Self-assembled nanoscale biosensors based on quantum dot FRET donors. *Nature Materials.* 2:630-38.

O'Connor, D.V., and D. Phillips. *Time-Correlated Single Photon Counting* (Academic, London, 1984).

Qdot™ Streptavidin Conjugates User Manual. (available online).

Willard, D.M., L.L. Carillo, J. Jung, and A. Van Orden. 2001. CdSe-ZnS Quantum Dots as resonance energy transfer donors in a model protein-protein binding assay. *Nano Lett.* 1:469-74.

Wu, X.Y., H.J. Liu, K.N. Haley, J.A. Treadway, J.P. Larson, N.F. Ge, F.Peale, and M.P. Bruchez. 2003. Immunofluorescent labeling of cancer marker Her2 and other cellular targets with semiconductor quantum dots. *Nature Biotechnol.* 21:41-6.

CHAPTER TWO

EFFECT OF SILICA NANOPARTICLE ARCHITECTURAL VARIATIONS ON THE PHOTOPHYSICAL PROPERTIES OF ENCAPSULATED FLUOROPHORES

INTRODUCTION

The need for fluorescent nanoparticles for use in biological and analytic applications is steadily increasing. Two approaches have been developed to meet these needs. In the first approach, the material itself is fluorescent, such as semiconductor nanocrystals (Larson *et al.*, 2003). In the second approach, fluorescent organic dyes are incorporated into some type of confining matrix (Nyffenegger *et al.*, 1993). Due to the plethora of organic dyes there is a strong possibility of developing many nanoparticles with a range of fluorescence characteristics, possibly far beyond the capabilities of quantum dots.

Stöber and coworkers (Stöber *et al.*, 1968) pioneered the method of embedding dye in silica nanoparticles. Since their work, a variety of nanoparticles ranging in size, composition, and architectures have been synthesized (Blaaderen, 1992, and Nyffenegger *et al.*, 1993).

Recently, the development of architectural variations on a basic core-shell fluorescent, monodisperse, silica nanoparticle morphologies has been described (Larson, 2004). In these particles, the core is composed of the organic dye tetramethylrhodamine isothiocyanate, TRITC, surrounded by a silica matrix, and it has been found that the presence of the silica shell altered the fluorescent properties (Ow

et al., 2003). Further experimentation revealed that the architecture of the core could be altered to achieve control of the photophysical properties of the nanoparticles (Larson, 2004).

With this motivation the architecture of the shell has now been altered to determine if this could also control the photophysical properties of the nanoparticles. In the present experiment, the expanded core-shell architecture from the work of Larson and Ow (Larson, 2004) was surrounded by increasingly thicker layers of the siliceous shell. Sixteen nanoparticles were synthesized, all of distinct sizes and their photophysical properties investigated. No correlation between the thickness of the silica shell and the brightness of the particle was found. However, as the size of the particle increased the siliceous shell acted as a protective coating for the TRITC dye in the center from potential quenchers allowing molecules to stay in the triplet state for longer periods of time.

MATERIALS AND METHODS

Synthesis of Expanded Core-Shell Morphology. All synthesis procedures were carried out by Hooisweng Ow in the Wiesner Laboratory at Cornell University. Dye precursor was synthesized by addition reaction between tetramethylrhodamine isothiocyanate (Molecular Probes) and 3-Aminopropyltriethoxysilane (Aldrich) in molar ratio of 1:50, in exclusion of moisture (Blaaderen, 1992). The core-shell synthesis protocols were modified from the classic Stöber protocol, similar to what was previously described by Nyffeneggar and co-workers as heterogeneous nucleation (Nyffeneggar, 1993). The expanded core-shell was synthesized by co-condensing an aliquot of tetraethylorthosilicate, TEOS, (Aldrich) with the dye-precursor in a reaction vessel with the appropriate amounts of ammonia, water, and solvent and allowed to react overnight. After the synthesis of the expanded core had completed, TEOS was

then added for the growth of the silica shell. After addition of each silica shell, made by the same amount of TEOS added at the same rate, and aliquot of the sample was removed for experimentation. This procedure was repeated a total of nineteen times although only sixteen of the additions were examined.

Fluorescence Correlation Spectroscopy, FCS. A mode-locked Ti:sapphire laser system (Tsunami; Spectra Physics), pumped by an Ar^{+}-laser (Spectra Physics), was used to generate femtosecond laser pulses in the 900nm range at repetition rate 80MHz and pulse width ~100fs. The beam was positioned with a Bio-Rad MRC 600 scanner coupled to a Zeiss Aviovert 35 inverted microscope and the sample excited through a 63x C-Apochromat water objective with NA=1.2 (Zeiss). The laser intensity was varied using a calibrated neutral density filter wheel (New Focus, Inc.). 2P-fluorescence was collected through the same objective and split from the excitation light with a 670nm long pass dichroic and passed through a HQ575_150 bandpass filter (Chroma). Filtered 2P fluorescence was imaged with a Hamamatsu GaAsP photomultiplier tube, PMT. The photon counts were autocorrelated using an ALV 6010 multiple tau correlator card. Once the autocorrelation had been recorded, the data was fit using a physical model where only experimental parameters were input (Larson, 2004). Residuals for FCS curves are the weighted residuals (Bevington and Robinson, 1992).

The autocorrelation function $G(t)$ is defined as $G(t) = < \delta F(t) \bullet \delta F(t+\tau) > / < F(t) >^2$, where $F(t)$ is the fluorescence obtained from the focal volume at time t, brackets denote ensemble averages, $\delta F(t) = F(t) - < F(t) >$, and τ is the delay. The FCS focal volume was calibrated using Alexa 488 as a standard. For an overfilled back aperture with an excitation wavelength of 900nm and 1.2 NA, the concentration calibration factor was 2.13nM/particle. The fitting function

is the standard function for one-component, three-dimensional diffusion (Thompson, 1991):

$$G(\tau) = \frac{1}{N}\left(1 + \frac{4D\tau}{w_{xy}^2}\right)^{-1}\left(1 + \frac{4D\tau}{w_z^2}\right)^{-1/2} \tag{2.1}$$

where w_{xy} and w_z are, respectively, the lateral and axial Gaussian 1/e width dimensions of the two-photon focal volume, N is the number of diffusing species in the focal volume, and D is the diffusion coefficient. At the excitation wavelength of 900nm, the lateral dimension was determined to be 250 nm and the axial dimension 640 nm (Larson, 2004).

Once the diffusing molecules are excited, some have the ability to undergo a spin conversion to the first triplet state (Lakowicz, 1999). Transition from the triplet state to the singlet ground state is forbidden, and, as a result, molecules tend to stay in the triplet state for a longer period of time than the first excited state. The fitting function for one-component, three-dimensional diffusion with a triplet fraction is (Thompson, 1991):

$$G(\tau) = \frac{1}{N}\left(\frac{1}{1-f}\right)\left(1 - f + fe^{\left(\frac{-\tau}{T}\right)}\right)\left(1 + \frac{4D\tau}{w_{xy}^2}\right)^{-1}\left(1 + \frac{4D\tau}{w_z^2}\right)^{-1/2} \tag{2.2}$$

where f is the fraction of diffusing species in the triplet state and T is the time spent in the triplet state.

Absorbance/Fluorescence. Absorbance measurements were done with a Cary 300 Bio UV/VIS dual beam spectrophotometer. Measurements were taken in 1nm step intervals from 350-750nm with a dwell of 1 sec on each interval. Fluorescence and excitation measurements were carried out on a PTI spectrofluorimeter. Excitation curves were collected from 350-600nm with the emission monochromator parked at 605nm. Emission curves were collected by exciting the samples at 514.5nm (position where the extinction coefficient of TRITC, ε_{TRITC}, is known) and collecting the

resulting fluorescence from 520-750nm. Again, measurements were taken in 1nm step intervals with a dwell of 1 sec on each interval and with a reference voltage of 1V.

RESULTS

The basic requirement for each shell layer is monodispersity in aqueous solution, which was determined by FCS measurements (Fig. 2.1). The goodness of fit to a one-component diffusion model is an accurate measure of monodispersity (Starchev *et al.*, 1999). The FCS curve provides two critical, independent parameters: the diffusion coefficient and the concentration (Eq. 2.1). The diffusion coefficient is directly related to the hydrodynamic radius (through the Stokes-Einstein equation), and the absolute concentration is important for quantifying photophysical parameters such as the brightness of the particle.

FCS curves of all the measured particles are shown in Figure 2.1. An incident laser power of ~0.9mW was used to excite the nanoparticles, and up to ~13.6mW was used to excite the TRITC sample. Progression from left to right at half the decay time illustrates the increasing size of the particles with the addition of shell layer by the increase in diffusion time. Figure 2.2 panel A graphically lists the results of the fit from Eq. 2.1 on the curves from Fig. 2.1. The diffusion coefficient has been transformed into the hydrodynamic radius (calculated as 22ºC), and here, as in Fig. 2.1, it is clear that there is an increase in the size of the particles.

The autocorrelation curve's amplitude relates the number of diffusing species, and the average count rate is a measure of the photons collected from the optically defined focal volume. The count rate per particle, CPP, for each diffusing species is thus attainable and is a direct measure of the brightness of the probe (Heikal *et al.*, 2001). Fig. 2.2 panel B relates the normalized brightness, to free TRITC, of the nanoparticles. Due to the fact that the nanoparticles were excited with a distinct power from TRITC

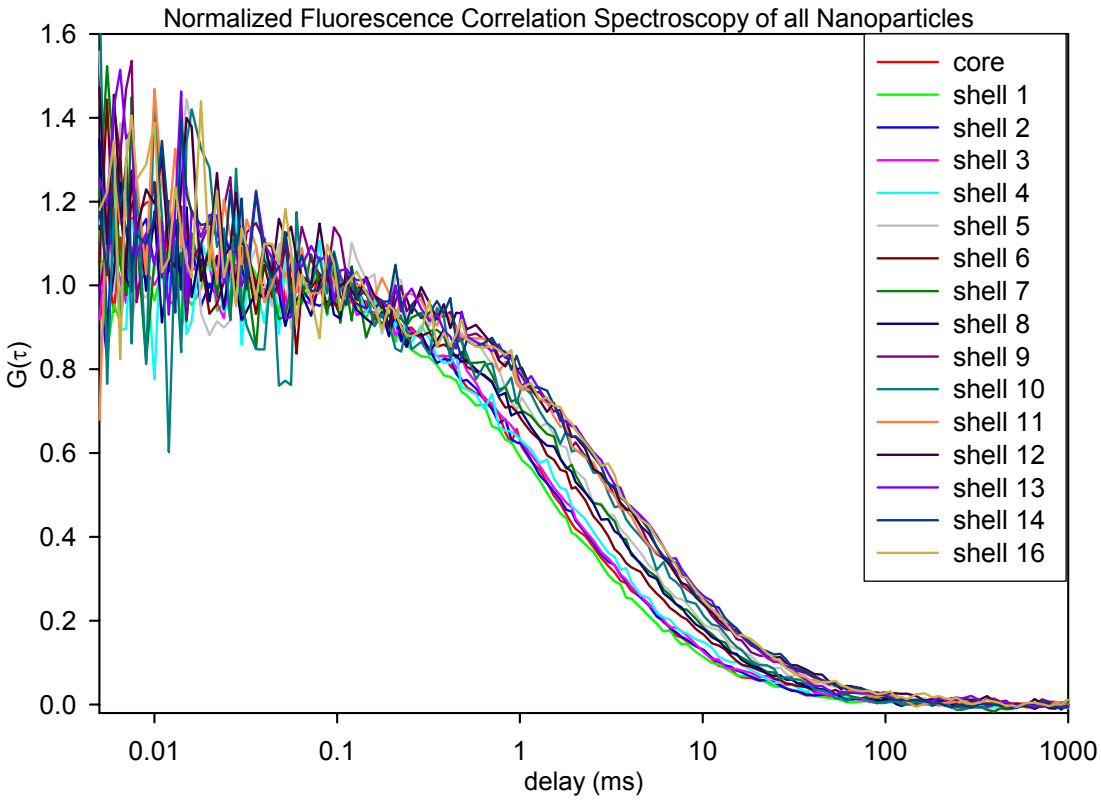

Figure 2.1: Normalized Fluorescence Correlation Spectroscopy of all nanoparticles. The measured nanoparticles from the core to addition of silica shell layer sixteen are shown above with the number of particles diffusing in the focal volume normalized to one. The concentration of each curve was normalized to one. This figure illustrates the increase in diffusion time, or the increase in size, with the addition of silica shell layers.

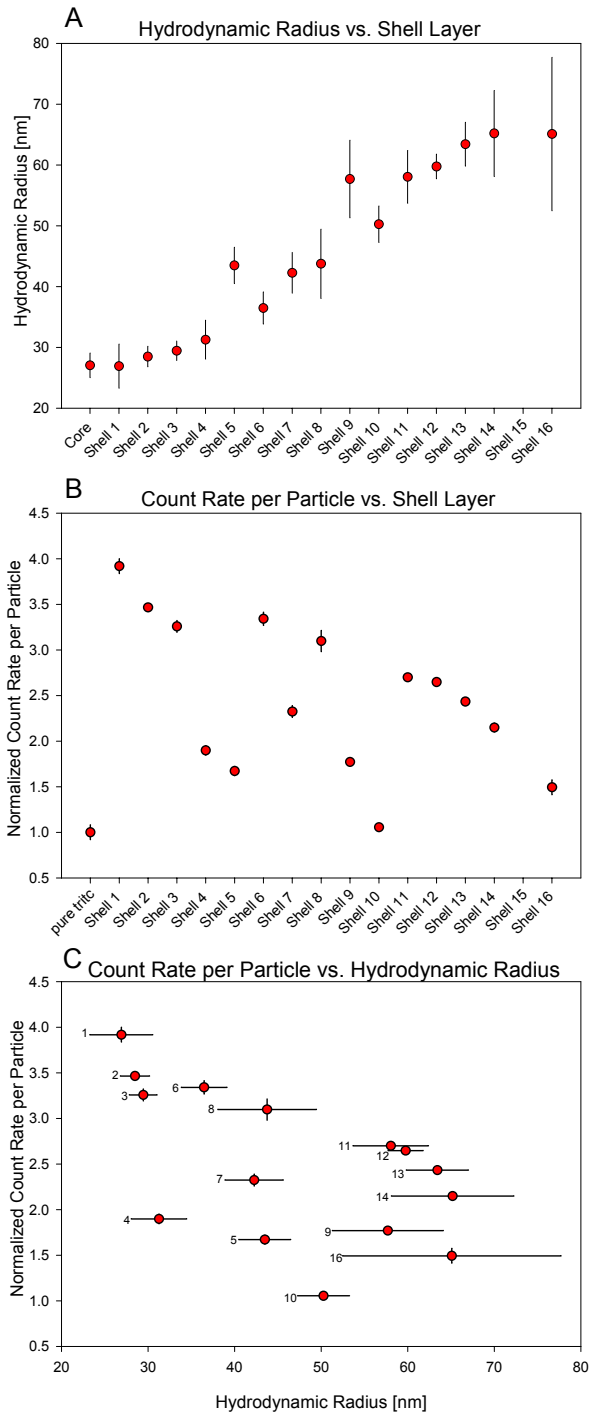

Figure 2.2: Radii and Count Rate Per Particle, CPP, Trends. Panels A-C are the compiled results from the FCS measurements. A) Radii vs. Shell layer. This panel illustrates the increase in radii of the nanoparticles as silica layers are added, as also shown in Fig. 2.1. B) CPP vs. Shell layer. Here the CPP of the nanoparticles is normalized to free TRITC. The CPP appears to remain relatively constant with respect to the shell layer with a wieghted average value of 2.2±0.1. C) CPP vs. Radii. Again normalized CPP values are used here. No trend appears evident in this panel.

the normalization no longer holds meaning, and the CPP is not a direct measure of the brightness. However, the science behind the trends remains valid even though the absolute value is without content. No persuasive trend appears in Fig. 2.2 B between the CPP and the shell layer. A weighted average CPP value of 2.2±0.1kHz/particle was found. Panel C in Fig. 2.2 illustrates the connection, or lack thereof, between CPP and hydrodynamic radius. Absolutely no trend is evident in this graph.

Since the CPP value is no longer a measure of brightness, an alternative method was used in order to elucidate this photophysical property of the nanoparticles. The brightness of the particle over the free TRITC dye was calculated with the number of TRITC molecules per particle and the relative quantum efficiency enhancement, QE enhancement, over free TRITC dye (Table 2.1, TRITC equivalents, QE enhancement, Brightness factor). A maximum of 3.3 QE enhancement over free dye was found for shell layer 6, while a minimum enhancement of 1.9 was found for shell layer 1 using the analysis presented below.

The number of TRITC molecules per particle can be determined through a combination of FCS and steady state absorbance measurements. By utilizing the concentration of the particles, as determined by FCS, and measuring a relative absorbance with respect to free TRITC, one can determine the number of TRITC equivalents in the particle and the quantum efficiency enhancement of the particle over free TRITC. Sample steady state measurements are shown in Figure 2.3 A-C. The absorbance was measured in real units of optical density, and the fluorescence is scaled relative to free TRITC, with the peak TRITC fluorescence set equal to the peak TRITC absorbance. The number of TRITC equivalents per particle, calculated using an extinction coefficient of $42{,}105 M^{-1}cm^{-1}$ at 514.5nm (Soper *et al.*, 1993), are complied in Table 2.1 along with the relative quantum efficiency enhancement over free TRITC.

As stated by Larson (Larson, 2004) the estimation of TRITC equivalents relies on the assumption that once TRITC has been incorporated into the particle there is no change in absorption. This assumption is not strictly valid (for example, Fig. 2.3 A), and even if it were the existence of non-fluorescing absorbance bands, as seen in Fig. 2.3 D-F, leads to wavelength-dependent quantum efficiency and TRITC equivalent value. For these three particles, the scaled absorbance (Fig. 2.3 D-F, red curve) is noticeably greater than the scaled excitation (Fig. 2.3 D-F, blue curve) at wavelengths less than 520nm. Hence it appears that photons that are absorbed at shorter wavelengths have a smaller probability of leading to fluorescence. The number of TRITC equivalents, Table 2.1 and Figure 2.4 A, was estimated by taking the observed optical density at 514.5 and dividing it by the expected optical density at that location. The weighted average TRITC equivalent for all silica shell additions is 12±3. This method of determination, however, overestimates the number of TRITC equivalents due to the weakly fluorescent bands at this wavelength, as is evident in Fig. 2.4 A.

The above measurements and calculations were only completed through silica shell addition 8. Starting at silica shell addition 7, large scattering components were found in the absorbance measurements making it impossible to determine the optical density contribution from the TRITC dye.

The product of the TRITC equivalents and the QE enhancement over the free dye is the brightness of the particle. Fig. 2.4 B compares the calculated brightness and the CPP for silica shell additions 1-8, while Table 2.1 lists the brightness factor. As can be seen in Fig. 2.4 B, the trend found for the CPP is the same as that found for brightness signifying that the science is the same—there is no correlation between thethickness of the silica shell and the brightness of the particle. Due to the overestimation of the number of TRITC equivalents, the value of the brightness factor should not be taken as absolute.

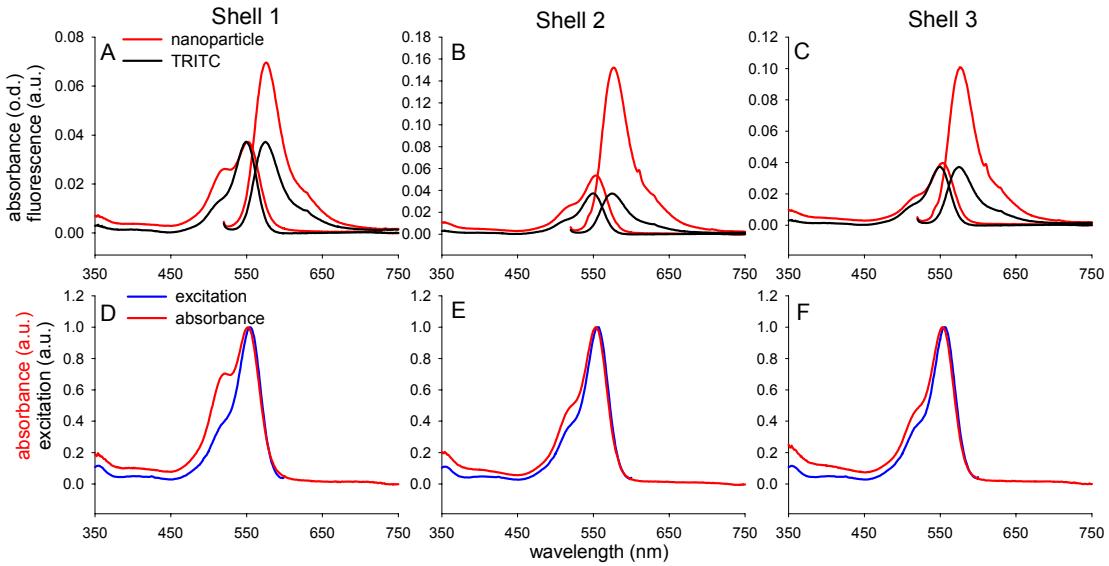

Figure 2.3: Steady State Spectroscopy of Nanoparticles. Panels A-C are the absorbance and fluorescence of the first three shell additions, respectively; shells 4-8 are not shown. The absorbance is in real units of optical density. The fluorescence is scaled relative to TRITC. Nanoparticle spectra is in red; TRITC spectra are in black. Panels D-F are the comparison between absorbance and excitation for the first three shell additions, respectively. Absorption spectra (red curves) are in units of optical density, and excitation spectra (blue curves) are scaled to the maximum of the respective absorbance. Note in panels D-F the existence of weakly fluorescing absorption bands.

Table 2.1: Brightness of Nanoparticles. Values are normalized to free TRITC in water. The TRITC equivalents were obtained from the absorbance at 514.5nm. The quantum efficiency enhancement is obtained from the difference in peaks relative to free TRITC. The brightness factor is simply a product of the TRITC equivalents and the QE enhancement.

Sample	**TRITC Equivalents**	**QE enhancement**	**Brightness Factor**
TRITC	1	1	1
Shell 1	16.7±0.6	1.9	31.6±1.1
Shell 2	11.7±0.2	2.8	32.8±0.66
Shell 3	11.7±0.3	2.5	29.2±0.85
Shell 4	11.1±0.5	3.0	33.2±1.5
Shell 5	7.1±0.3	2.7	19.1±0.79
Shell 6	10.1±0.3	3.3	33.3±1.0
Shell 7	10.6±0.5	2.7	28.7±1.5
Shell 8	13.8±0.6	2.5	34.4±1.5

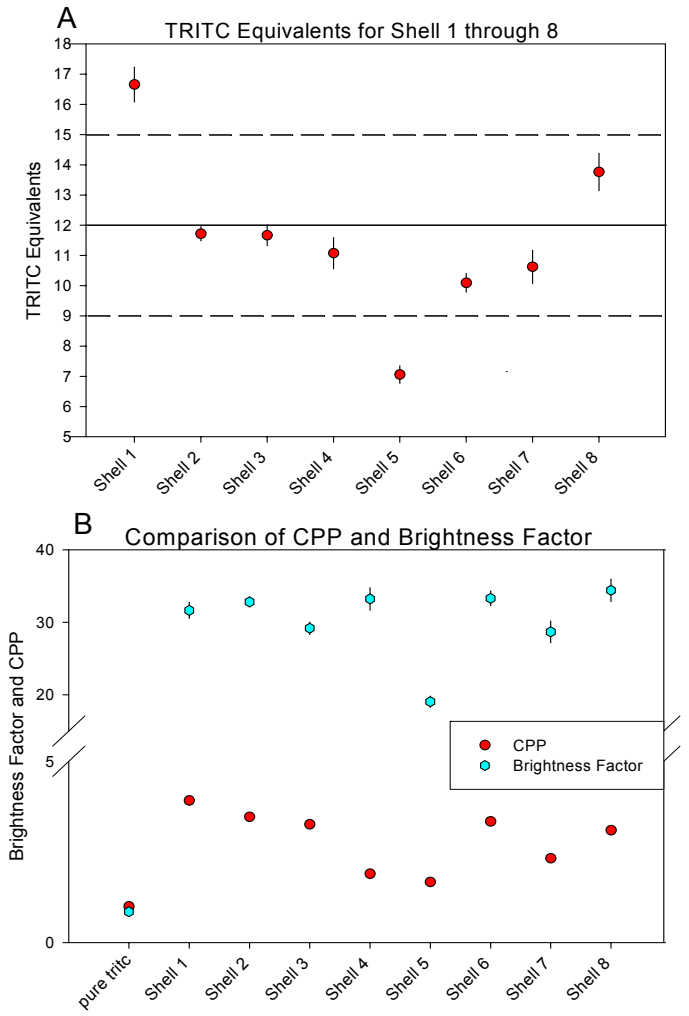

Figure 2.4: TRITC Equivalence and CPP vs. Brightness. A) TRITC Equivalents. Shown is the weighted average TRITC equivalent for the synthesis, 12±3, along with the individually calculated TRITC equivalents for each shell layer. This calculation could be done only through shell 8 due to excessive light scattering in absorption measurements for the higher radii particles. As seen in Fig 2.3 shell 1 has a large non-fluorescing absorption band at 514.5nm, and hence the estimation of the TRITC equivalent in this case is poor. B) Comparison of CPP and Brightness. The trend for brightness factor and CPP is the same for the nanoparticles that were able to be measured. The actual numerical values are distinct for reasons discussed in the text.

As the silica shell addition increased, evidence of the occupation of the triplet state appeared. The TRITC molecule is known to strongly express a triplet state, and hence the appearance of the triplet state in the nanoparticles is not surprising. Determination of the triplet state requires a power dependence study; as incident power levels are increased occupation of the triplet state also increases, however, the time spent in the triplet state is not expected to change. Incident powers in the range of ~0.9-5mW were used to excite shell layers 9-16. All shell layers investigated were found to exhibit the triplet state by demonstrating an increased occupation of the triplet state with constant triplet time occupation for increasing incident powers. The autocorrelated curves were fit with Eq. 2.2 yielding the fraction of occupation and triplet time parameters along with the diffusion coefficient and concentration. The triplet times obtained at each incident power were used in a weighted average to produce Figure 2.5 A. As can been seen in Fig. 2.5 A, there is a clear trend towards longer occupation of the triplet state as shell layers are added. Since the existence of highly protected environments are known to lead to triplet state occupation (Lacowicz, 1999), it appears that the shell layers are sheltering the TRITC dye from potential quenchers, such as dissolved oxygen, thus allowing the TRITC molecule to remain in the triplet state for longer periods of time. At a single incident power level (in this case ~0.9mW) the degree of occupation in the triplet state appears to remain constant as shown in Fig. 2.5 B. Due to the large error associated with these measurements it is difficult to determine the existence of a trend that was simply not resolvable here.

DISCUSSION

It has been demonstrated that architectural variations on the shell of the expanded core-shell morphology result in no tractable change in the photophysical properties of TRITC dye, silica encapsulated nanoparticles. However, these variations

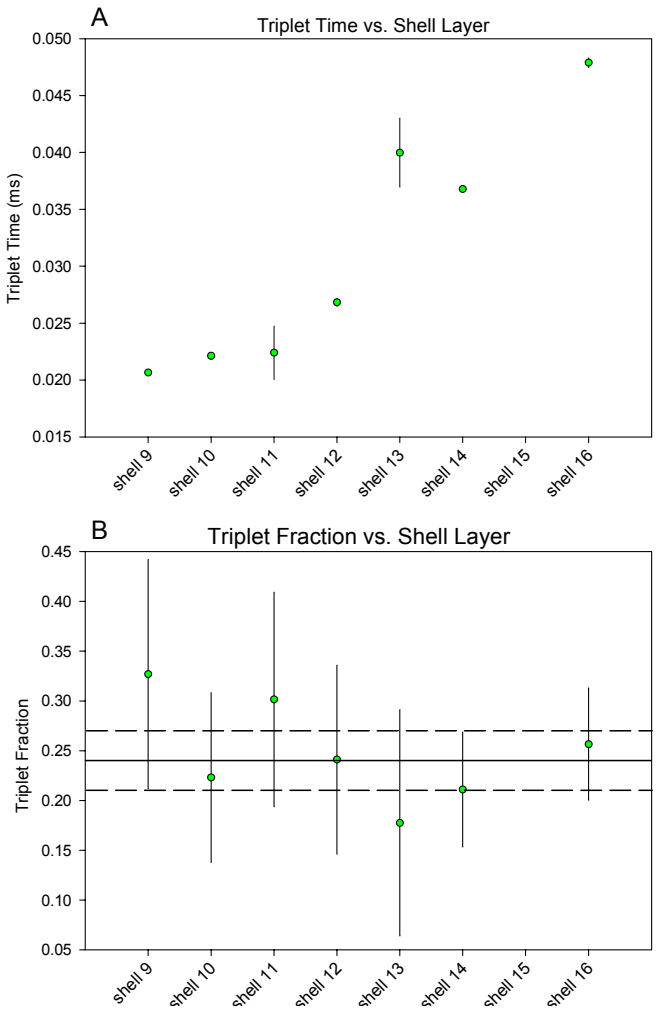

Figure 2.5: Triplet Investigation. Panels A-B are the complied results from a set of triplet studies done on shell layers 9 through 16. A) Triplet Time vs. Shell layer. The triplet time value is a weighted average of the triplet times obtained for a series of incident laser intensities. Here the trend towards longer triplet times as additional shell layers are added is evident. B) Triplet Fraction vs. Shell Layer. The triplet fraction series has been calculated for one incident laser intensity. No trend appears to exist between the fraction of particles in the triplet excited state and the shell layer; the average fraction for all shell layers at one incident intensity is 0.24±0.03. However, due to the large error associated with these measurements, it is possible that there is a trend that was not resolvable here.

have shown to act as a shield for the TRITC molecules from potential triplet state quenchers. Hence, it may be possible to make precisely controlled nanoparticles of specified triplet state dwell times.

Note that the core is of the same size as the first two shell layers (Fig. 2.2 panel A), a finding distinct from that of Larson and Ow (Larson, 2004). These particles were synthesized a few months before final measurements were taken. Due to this fact, the additional silica in solution with the core particle condensed around the core making it of similar size and photophysical property of the first shells. A brand new core was synthesized at this point to corroborate the above reasoning. The new core synthesis was smaller in size and also had a decreased brightness factor and decreased count rate per particle, thus confirming the hypothesis and conforming to the previous work of Larson and Ow (Larson, 2004).

Panel D in Fig. 2.3 has a strong non-fluorescing band reminiscent of the band in the compact core-shell architecture explored by Larson and Ow (Larson, 2004). The QE enhancement for this particle, 1.9 (Table 2.1), is also close to the enhancement seen by Larson and Ow for the compact core-shell morphology. Again, it is possible that due to the time lapse between synthesis and final measurement that the intended morphology changed.

Within the context of the work done by Larson and Ow (Larson, 2004), the relative decrease in the quantum efficiency enhancement for the expanded core-shell architecture over free TRITC, Tabel 2.1, makes complete sense. For Larson and Ow, the quantum efficiency enhancement for the different architectures was due to the decrease in the non-radiative rate of the silica particles. It was found that the cause of the variation in the non-radiative rate was due to the hindered rotation of the dye molecules within the silica matrix (Larson, 2004). The particles that Larson and Ow were working with were considerably smaller, in fact particles of the same size have

yet to be reproduced. Thus, it is likely that this larger core did not confine the dye to the extent done before, hence allowing more rotation within the silica matrix and thus increasing the non-radiative rate and decreasing the quantum efficiency enhancement.

CONCLUSION

The construction of silica nanoparticles in varying morphologies has achieved modified photophysical properties of the encapsulated dyes in the past. It has been found that the thickness of the shell protects the organic dye from potential quenchers, such as oxygen, allowing the dye to remain in the triplet state for longer periods of time. The brightness of the particles has now been found not to depend upon the thickness of the siliceous shell. However, the ability to design these particles for specific properties shows great promise for their future use in biological applications.

REFERENCES

Bevington, P.R., and D.K. Robinson. 1992. Data Reduction and Error Analysis for the Physical Sciences. McGraw-Hill, Inc., New York.

Blaaderen, van A., and A. Lvrij. 1992. Synthesis and Characterization of Colloidal Dispersions of Fluorescent, Monodisperse Silica Spheres. *Langmuir*. 8:2921-31.

Heikal, A.A., S.T. Hess, and W.W.Webb. 2001. Multiphoton molecular spectroscopy and excited state dynamics of enhanced gree fluorescent protein (EGFP): acid-base specificity. *Chem. Phys.* 274:37-55.

Lakowicz, J.R. *Principles of Fluorescence Spectroscopy* 2nd edn (Kluwer Academic, New York, 1999).

Larson, D.R., W.R. Zipfel, R.M. Williams, S.W. Clark, M.P. Bruchez, F.W. Wise, W.W. Webb. 2003. Water-Soluble Quantum Dots for Multiphoton Fluorescence Imaging in Vivo. *Science.* 300:1434-36.

Larson, D.R. (2004). Dissertation: Optical Approaches to the Study of Nanoparticles and Biology: Quantum Dots, Silica Dots, and Retroviruses. Cornell University. Chapters 1 and 4.

Nyffenegger, R., C. Quellet, and J. Ricka 1993. Synthesis of Fluorescent, Monodisperse, Colloidal Silica Particles. *J. Colloid Interface Sci.* 159:150-57

Ow, H., D.R. Larson, P. Sengupta, B.A. Baird, W.W. Webb, and U. Wiesner. 2003. Core-Shell Fluorescent Silica Nanoparticles for Biological Imaging. *Angew. Chem. Int. Ed.* submitted.

Soper, S.A., H.L. Nutter, R.A. Keller, L.M. Davis, and E.B. Shera. 1993. The Photophysical Constants of Several Fluorescent Dyes Pertaining to Ultrasensitive Fluorescence Spectroscopy. *Photochem. Photobio.* 57:972-77.

Starchev, K., J. Buffle, and E. Pérez. 1999. Applications of Fluorescence Correlation Spectroscopy: Polydispersity Measurements. *J. Colloid Interface Sci.* 213:479-87.

Stöber, W., A. Fink, and E. Bohn. 1968. Controlled Growth of Monodisperse Silica Spheres in Micron Size Range. *J. Colloid Interface Sci.* 26:62.

Thompson, N.L. 1991. Fluorescence Correlation Spectroscopy. Plenum Press, New York. 337-378 pp.